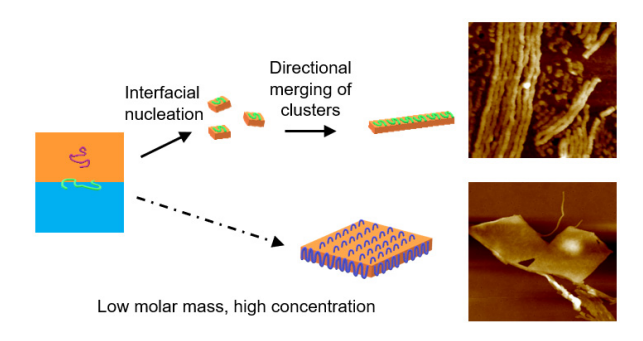
# Tuning Poly(L-Lactic acid) Crystallization Pathways via Evaporative Crystallization on Water Surface

Qian Qian, Shichen Yu, Christopher Y. Li\*

Department of Materials Science and Engineering, Drexel University, Philadelphia,

Pennsylvania 19104, United States



KEYWORDS: Polymer crystallization, polymer single crystals, evaporative crystallization, water surface, Langmuir-Blodget film

# ABSTRACT

Evaporation-induced structures in soft matter have been extensively studied. Recent work showed that evaporative crystallization on water surface (ECWS) provides a unique approach to tuning polymer crystallization pathways. In this work, we report the crystallization behavior of poly(L-lactic acid) (PLLA) using ECWS. The structure and morphology of the crystallization process were followed by atomic force microscopy and transmission electron microscopy. Results show that both one-dimensional (1D) crystalline filaments and two-dimensional (2D) lamellae form in ECWS, highlighting the complex crystallization pathways. Detailed analysis confirms that the 1D crystals are formed by interfacial crystallization, while 2D crystals form at the later stage of the evaporation process when the polymer centration in solution is high. Crystalline morphology can be tuned by polymer concentration, molecular weight, and crystallization temperature. Our work demonstrates that ECWS is a powerful crystallization method to understand and tune polymer crystallization pathways.

## Introduction

Liquid-liquid interfaces can provide soft confinement to polymer chain crystallization and alter the crystallization pathway and kinetics. 1-9 They offer a powerful tool for tuning

crystallization for morphology control and materials' properties. Confined crystallization involving a liquid-liquid interface has been reported in polymer blends and solutions. <sup>1-10</sup> It was shown that the curved interface of miniemulsion droplets can direct polymer crystallization to form a class of crystalsomes. 10-16 Confinement effects have been observed in two-dimensional (2D) Langmuir-Blodgett (LB) polymer films using water as the subphase. 17-23 Polymers that have been investigated include polycaprolactone (PCL), <sup>17-19, 24, 25</sup> poly(i-methyl-methacrylate) (iPMMA),<sup>20, 21, 26</sup> poly(L-lactic acid) (PLLA),<sup>22, 23, 26-29</sup> poly(D-lactic acid) (PDLA),<sup>27</sup> poly(ethylene) (PE),<sup>30</sup> block copolymers (BCP),<sup>31,32</sup> etc. Polymer crystallization in LB systems depends on the polymer's chemical structure and the compressing speed. In the case of PCL, some of the carbonyl groups in the amorphous region detach from the air-water interface during compression, and the chain folds back at the ester linkage. This results in a vertical orientation of the PCL chains to the air-water interface, forming a "flat-on" lamellae on the water surface where the 2D crystals are parallel to the water surface.<sup>24</sup> Direct monitoring crystals on the water surface by grazing incidence wide-angle X-ray scattering and infrared reflection absorption spectroscopy demonstrated that PCL chains are tilted from the water surface normal, suggesting that the vertical chain orientation previously observed might be due to film transfer.<sup>25</sup>

In PLLA and iPMMA crystallization on LB films, the polymer chains stay parallel to the water surface during crystallization on the water surface. Esker *et al.* reported that PLLA could form a crystalline monolayer on the water surface as an LB film. PLLA molecules adapt a 10<sub>3</sub>

helices conformation over nearly the entire length of the polymer chain, forming an extended-chain crystal (ECC).<sup>22, 23</sup> This was later confirmed by Kumaki and coworkers using high-resolution Atomic Force Microscopy (AFM).<sup>27</sup> They reported that the lamella thicknesses are proportional to the molecular weight, and the chains are tilted counterclockwise and clockwise for (PLLA) and (PDLA). Kressler *et al.* compared the crystallization behavior of PCL, PLLA, and iPMMA. They suggested that the chain orientation of PCL and PMMA depends on the chain stiffness instead of the interaction with the water surface.<sup>24</sup> PMMA has a longer persistence length than PCL and, therefore, has a higher tendency to remain parallel to the water surface.<sup>13</sup> Recently, Reiter *et al.* demonstrated the importance of controlling the compressing speed on the crystallization pathways of PLLA nucleation and morphology.<sup>28, 29</sup> Yang *et al.* investigated the crystallization behavior of a series of giant surfactants.<sup>33, 34</sup> They further reported the observation of fractal crystal morphologies in LB films. <sup>33, 34</sup>

Evaporation-induced structures in soft matter are complex and can be tuned by the competition between the time scales of solute diffusion and solvent evaporation ( $\tau D$ ,  $\tau EV$ , and their ratio, the Peclet number  $Pe = \tau D/\tau EV$ ). Polymer evaporative crystallization has been investigated in thin films and sessile droplets. Recent computer simulations demonstrated that fast evaporation (Pe > 1) can induce 2D polymer crystallization within the skin layer at suitable temperatures and evaporation rates. Evaporative polymer crystallization on a water surface (ECWS) has recently been developed as a simple method to understand the polymer crystallization process on the water surface and to prepare Janus single crystal films. In this

method, an aliquot of polymer solution is drop-cast on water surfaces. The solution is then spread on the surface with a small, finite thickness (microns). Polymer crystallization occurs as the solvent is evaporated. This process can be viewed as a different and complementary crystallization method to the established crystallization in LB films, and there are at least five significant attributes of ECWS. 1) ECWS deals with a quasi-2D system compared with a 2D monolayer in LB. The organic phase (polymer solutions) can be easily varied from tens to millions of Rg of the polymer, offering ample parameter space for crystallization study. 2) The crystallization kinetics can be easily controlled by tuning the solvent evaporative rate; seconds to days of evaporation/crystallization time are attainable. 3) Different from LB, where polymer films are compressed laterally and parallel to the water surface, the phase front in ECWS progresses orthogonal to the solvent/water interface. 4) No lateral pressure is applied in ECWS, eliminating the potential compression effect on polymer crystallization.<sup>25</sup> 5) The ECWS can be programmed by varying the polymer concentration, temperature, evaporation rate, surface tension, polymer chain structure, etc. Furthermore, the water surface is more dynamic compared to solution-cast crystallization onto a hydrophilic solid surface. It allows facile diffusion and crystallization of adsorbed polymer chains at the liquid/liquid or liquid/air interface. Therefore, ECWS is a versatile platform to study polymer crystallization.

## Results and Discussion

Our previous work reported the ECWS of PCL with well-defined chain end groups. <sup>41</sup> The strong interaction of the water surface and the COOH chain ends of PCL plays a crucial role in PCL crystallization. In the case of telechelic COOH-PCL-COOH, millimeter-scale, 2D, flat-on PCL lamellar single crystals are formed. *In-situ* water nanocondensation experiments using environmental scanning electron microscopy demonstrated that all the COOH groups are located at the PSC-water interface, and the resultant 2D PSC is Janus. Herein, we report on the ECWS of PLLA. While 1D crystalline PLLA ribbons were demonstrated in the LB systems, we show in this work that a biphasic structure of 2D and 1D PLLA crystals is formed in ECWS. ECWS conditions such as polymer concentration, evaporation/crystallization temperature, and the polymer molecular weight (MW) can control this biphasic morphology. The formation mechanism of 1D and 2D PLLA crystals will be presented.

In a typical ECWS process, 1g of toluene was added atop 80 mL water in a 100 mL glass beaker to create a  $\sim$  632 µm thick organic phase on the water surface. An aliquot of 0.03 wt.% PLLA (molar mass 10 kDa, dispersity D=1.1) /toluene stock solution was drop-wisely added to the toluene phase, generating a 1.95 x  $10^{-4}$  wt.% PLLA/toluene solution. Such a concentration is selected as the complete evaporation of the toluene phase would lead to a thin PLLA layer on the water surface with a thickness of  $\sim$ 1.66 nm (see supporting information). In our experiment, the toluene evaporated over a period of time (from three to 10 h; see **Figure S1** for the evolution of organic phase thickness, polymer concentration, and the solvent mass

loss during the ECWS) controlled by forced nitrogen flow (typically at 50 SCCM) and temperature (Figure 1a). Upon completing the evaporation, the film on the water surface was collected using a Blodget-Schaefer-type method using a pre-cleaned glass slide, and atomic force microscopy (AFM) was used to examine crystalline morphology. Figure 1b shows the PLLA crystals observed using the PeakForce Tapping mode after evaporating 15 µL of the PLLA solution at 21 °C for seven h. The AFM height image shows both 1D ribbons and 2D lamellae morphologies. The 1D ribbon is rigid and bent at a sharp angle. The width and height of the ribbon are approximately 40-80 nm and 12 nm, respectively. A large flat-on, lozengeshaped crystal is also seen. The lamella has a thickness of 12 nm, and two of the edges are (partially) covered by PLLA 1D ribbons. TEM bright field image and selected area electron diffraction (SAED) of the two types of crystals are shown in Figure 1c-d. A typical [001] zone diffraction pattern is observed for the 2D lamellae, confirming the 2D crystals are flat-on α phase PLLA lamellae with an orthorhombic unit cell of a = 1.0683 nm, b = 0.6170 nm and c (chain axis) = 2.8860 nm. <sup>42</sup> For the 1D ribbon, only a pair of (110) diffractions were observed along the ribbon axis. This suggests that the long axis of the ribbon is perpendicular to the (110) plane based on the α PLLA unit cell. In the 1D crystal, the PLLA chains are perpendicular to the ribbon's long axis. They also parallel the water surface upon crystallization (Figure 1e-f).

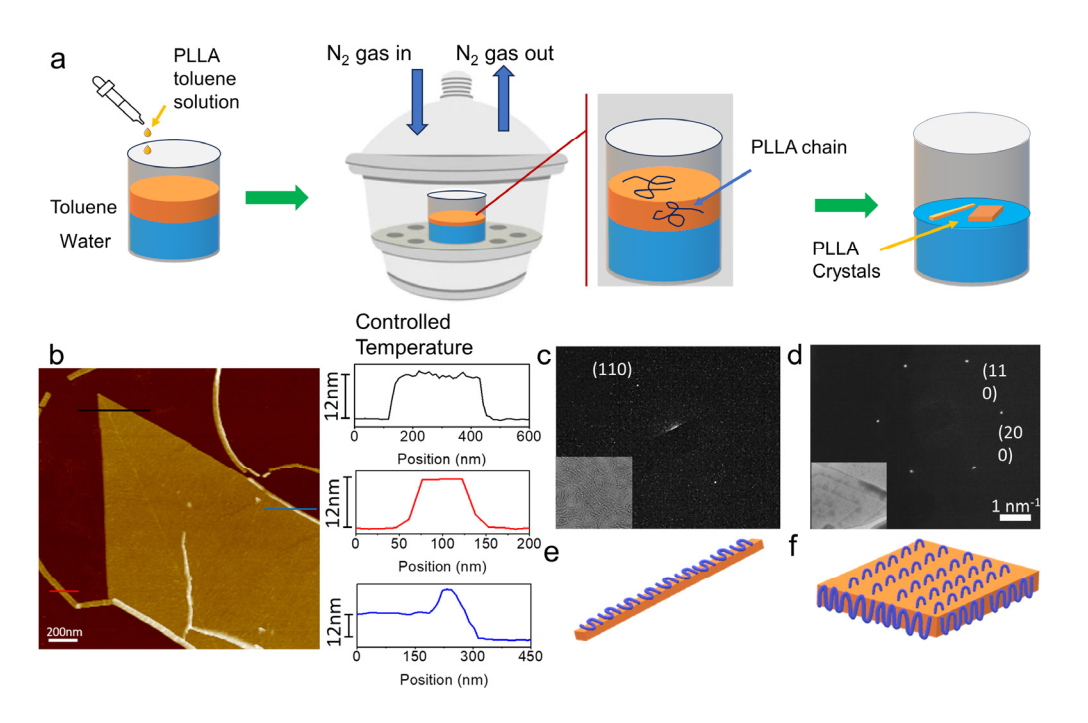


**Figure 1.** Evaporative crystallization of PLLA on water surface. (a) Schematic illustration of the experimental procedure. (b) An AFM height image of the biphasic morphology of PLLA formed by evaporating 15  $\mu$ L of the PLLA toluene solution at 21 °C for seven h on water surface. Both 1D ribbon and 2D lamellar morphologies can be seen. Right panels show the corresponding height profiles. (c) and (d) are the selected electron diffraction patterns of PLLA ribbons (c) and 2D lamellae (d). The insets in (c) and (d) are the corresponding morphologies. (e-f) Schematics of a 1D ribbon and a 2D lamellae, respectively. In the ribbon, the polymer chains are parallel to water surface and perpendicular to the ribbon axis. In the 2D lamellar, polymer chains are perpendicular to the water surface.

Flat-on (2D) and edge-on (1D) crystals are formed in the ECWS process of PLLA. This biphasic morphology is in stark contrast to the ECC observed in the LB system, where only 1D PLLA crystals are seen with a thickness of only ~0.86 nm, corresponding to a single layer of

the ECC and a crystal width of  $\sim$  80% of the extended chain length. Since PLLA adopts a  $10_3$  helical conformation in the unit cell, the projected distance per repeating unit along the chain axis is  $2.8860/10 \sim 0.289$  nm. For a 10 kDa PLLA, an extended chain would be  $\sim 40$  nm. Therefore, the observed 1D ribbon is wider and thicker than the thin ECC in LB. Furthermore, the previously suggested chain tilting in ECC is absent in ECWS, as evidenced by the SAED results: in the 1D ribbon, chains are perpendicular to the ribbon axis.

The observed biphasic morphology indicates that ECWS significantly alters the polymer crystallization pathway compared with solution crystallization or crystallization in an LB system. In the ECWS, a sub-millimeter-thick polymer solution evaporates on a water surface, and polymer chains could be pinned at the solvent-water interface followed by crystallization. Once polymer crystals are formed at the interface, free polymers can be supplied to the crystal growth front via the interface or the bulk organic solution. Furthermore, since polymer concentration gradually increases as the solvent evaporates, crystallization in the solution could also occur as it reaches the saturation concentration. To decipher this complex process, we first estimate the rate of polymer absorption to the interface after adding the PLLA solution to the top toluene phase. To this end, a large toluene/water interface was created using 62 g toluene and 800 mL water in a 1 L beaker. A Wilhelmy plate was immersed in the liquid phase to monitor the interface tension change (see Figure S2). Calculated amounts of PLLA solution were added to the toluene phase. As shown in Figure 2a, within 2 seconds (see the enlarged figure of the  $\Pi$ -A isotherm, **Figure S3**) of introducing the PLLA solution, the interface tension

changed by 3.0, 3.8. 4.0, 5.0, 6.0, 6.9 mN/m for total PLLA concentrations of 0.13, 0.26, 0.43, 0.65, 1.3, 1.95 x  $10^{-4}$  wt.%, respectively. The interfacial pressure was then stabilized. This indicates that PLLA chains can be quickly absorbed onto the toluene/water interface. The time scale (< 2 s) is negligible compared to the crystallization time (~three - 10 h) used in this study.

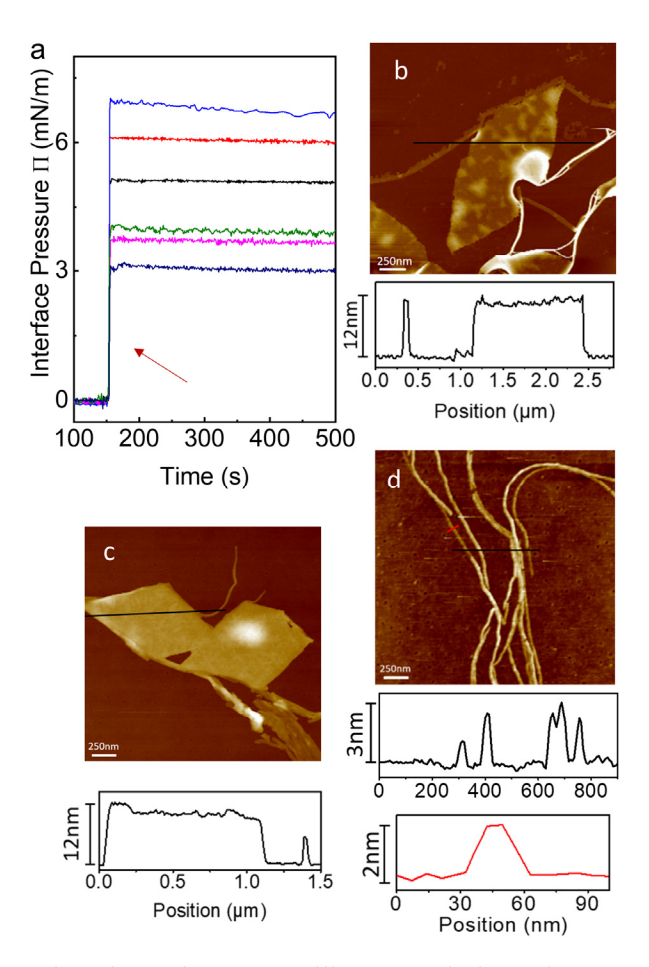


**Figure 2.** Concentration-dependent crystalline morphology in ECWS. (a) Interfacial pressure upon introducing PLLA solutions (from bottom to top, 0.13, 0.26, 0.43, 0.65, 1.3, 1.95 x  $10^{-4}$  wt.%, respectively), measured using the Wilhelmy plate method. (b-d) AFM height images and the corresponding height profiles of the PLLA crystals obtained by ECWS using (b) 10, (c) 5, and (d) 2  $\mu$ L PLLA solution at 21 °C for seven h.

Next, since a smaller amount of polymer chains in the starting solution should lead to increasingly insignificant solution crystallization, we reduced the initial amount of PLLA solution from 15  $\mu$ L to 10, 5, and 2  $\mu$ L, corresponding to an initial PLLA concentration of 1.95, 1.30, 0.65, and 0.26 x10<sup>-4</sup> wt.%, respectively. The same ECWS procedure was followed, and **Figure 2b-d** shows the corresponding crystal morphology. Biphasic crystals are again seen in **Figure 2b-c** when 10 and 5  $\mu$ L solutions are used. The 1D ribbons are thinner (~ 9 -12 nm). The thickness of the 2D lozenge crystals is similar (12nm) to **Figure 1**. In the 2  $\mu$ L sample, however, only thin 1D filaments are observed. These filaments seemingly differ from the 1D ribbons in **Figure 1b**, as they appear more flexible and thinner (1.5-3 nm thick). The results strongly suggest that the 2D lozenge lamellae in ECWS are formed when more polymer molecules are available. Note that the width of these 1D filaments is less than the contour chain length of 10 kDa PLLA (~40 nm), indicating that a folded chain instead of ECC is formed in the 1D filament.

To better understand the crystal formation process in ECWS, the temporal evolution of the crystals was captured by collecting samples at a crystallization time of 1h, three h, four h, six h, and seven h for the 5  $\mu$ L sample, as shown in **Figure 3**. At one h crystallization time, small round aggregates can be seen in the AFM height image, with an average height of 1.5-2 nm and  $\sim$  25 nm lateral sizes. At three h, anisotropic and elongated aggregates can be seen, up to 14 nm high and 100 nm long. Still, the morphology is dominated by the isotropic round aggregates with a slightly increased average size ( $\sim$  2-3 nm high and 40-50 nm wide). The

morphology dramatically changes at the four h growth time. As shown in **Figure 3c**, the image is covered by 1D filaments that are tens of micrometers long, with a uniform thickness and width of 1-3 and 26nm, respectively. The filaments are locally aligned, forming a smectic-like packing on the surface. In the background, smaller filaments (~ 1 nm thin) correspond to monolayers of PLLA crystals and appear to align longitudinally. Similar 1D morphology is seen at five h growth time (Figure 3d), while at 6 and 7 h, the biphasic morphology consisting of 1D filaments and 2D lamellae is seen. The filaments are thicker than those observed in **Figure 3c-d** ( $\sim 6$  nm vs. 3 nm), and the lamellae are also  $\sim 6$  nm thin. The biphasic morphology is similar to those observed in Figure 1b and Figure 2b-c. Note that both lozenge-shaped and irregular 2D lamellae are seen. Interestingly, the 2D lamellae show a thickness of 6 nm, which is thinner than the 12 nm thick 2D crystals in Figure 1-2. In Figure 3e-f, samples were dried at an elevated temperature (60 °C), while previous samples were dried at 21 °C. Higher drying temperatures lead to shorter drying times. The 2D crystals might have thickened more during the lower-temperature drying process and exhibited greater thickness. Our future study will systematically investigate the Annealing effect of ECWS crystals.

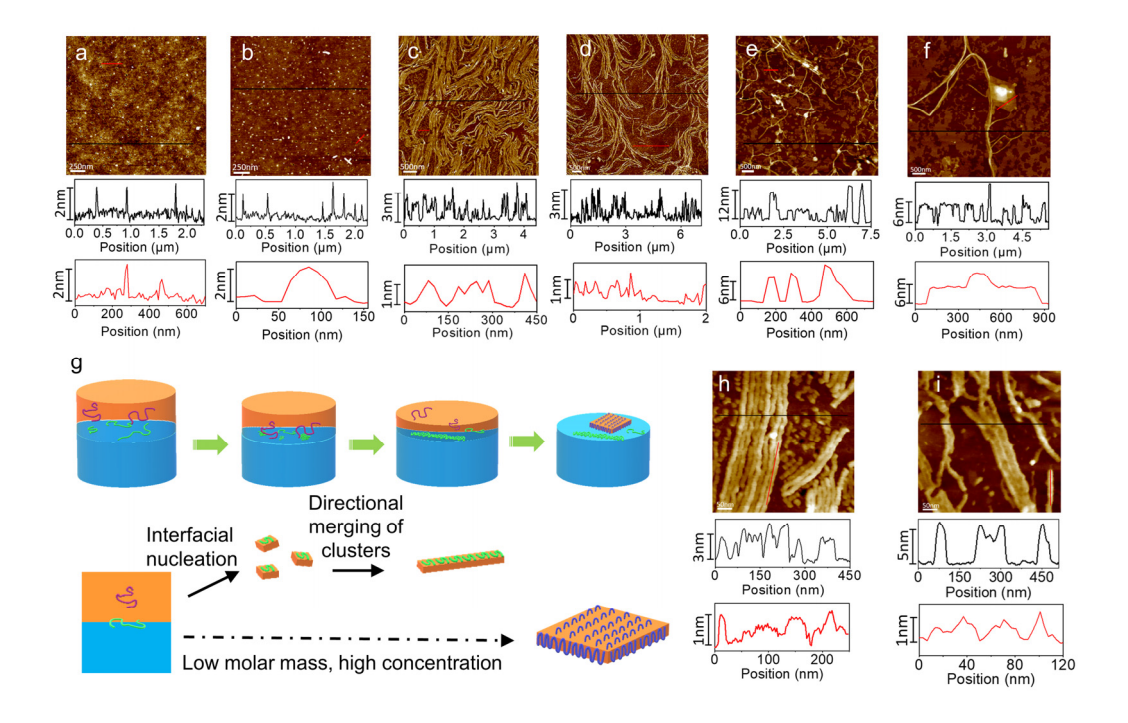


**Figure 3.** Formation mechanism of 1D and 2D crystals in ECWS. (a-f) AFM images and the corresponding height profiles of PLLA crystals formed using 5μL of 0.03 wt % PLLA 10 kDa toluene solution on water surface after (a) 1 h, (b) 3 h), (c) 4 h, (d) 5 h, (e) 6 h, and (f) 7 h of crystallization. (g) schematic illustration of the morphology evolution. Green chains are pinned at the water-toluene interface and purple chains are in the toluene phase. (h-i) displays the enlarged images of (c-d) with the height profiles, highlighting the rough and periodic nature of the 1D filaments.

Based on the above observation, we can propose the evolution of the 1D and 2D crystalline morphologies in the ECWS process, as shown in **Figure 3g**. PLLA chains are first quickly absorbed onto the toluene-water interface. They gradually form round clusters with a thickness of 1.5 nm. These clusters serve as the nuclei for the following crystallization process. Note that the thickness of the clusters (nuclei) is approximately twice that of the ECC crystals formed in the LB system (0.86 nm), indicating the formation of a bilayer structure. This can be attributed to the weaker confinement effect of the toluene/water interface compared with the air-water

interface (surface tension of 35 vs. 72.8 mN/m) and the presence of a polymer toluene phase atop water. As the toluene evaporates, the polymer concentration in the toluene phase increases, leading to an increased PLLA concentration at the toluene-water interface. After the critical concentration is reached, crystallization at the interface occurs. Further evaporation of the solvent leads to the growth of the filament along the longitudinal and transverse directions, and the filaments become thicker and wider. Figure 3h-i displays enlarged images of Figure 3c-d, which reveal rough edges and periodical height changes along the filaments. This suggests that the 1D filaments were formed by merging small PLLA clusters, which mimics the particlemediated crystal growth mechanism. 43-47 Note that clusters similar to Figures 3a,b also form when noncrystalline poly(L,D-lactic acid) is used (Figure S4). However, they do not evolve into 1D or 2D objects due to the lack of crystallization. Figure 3h-i also suggests that lateral merging of the filaments is feasible. Note that solution crystallization away from the interface could occur as the PLLA concentration in the toluene phase increases. This may also be induced (nucleated) by the 1D filaments at the toluene/water interface. Growing in the bulk toluene phase alleviates the confinement effect, resulting in the classical lozenge-shaped crystals. Due to the extremely low polymer concentration, solution crystallization would only occur at the end of the evaporation process, where the bulk solution centration approaches the saturation concentration of PLLA at room temperature (Figure S1).

Of interest is to compare the chain orientation in ECWS with the 1D confined polymer crystallization in semicrystalline BCPs. Homogeneous and homeotropic crystal orientations,

where polymer chains are respectively parallel and perpendicular to the interface, have been observed in lamella phase BCPs, and the crystal orientation depends on Mw and  $T_c$ . <sup>48-50</sup> It was proposed that the homeotropic chain orientation is thermodynamically more stable, while high nucleation density at high undercooling could lead to homogeneous orientation due to the collective crystal orientation adjustment. Similar homeotropic orientation was also observed in BCP crystalsomes formed in miniemulsion crystallization. <sup>15</sup> The parallel chain orientation in the ECWS, however, is due to the pinning of the PLLA chains onto the interface, which is categorically different from the BCP homogeneous crystal orientation.

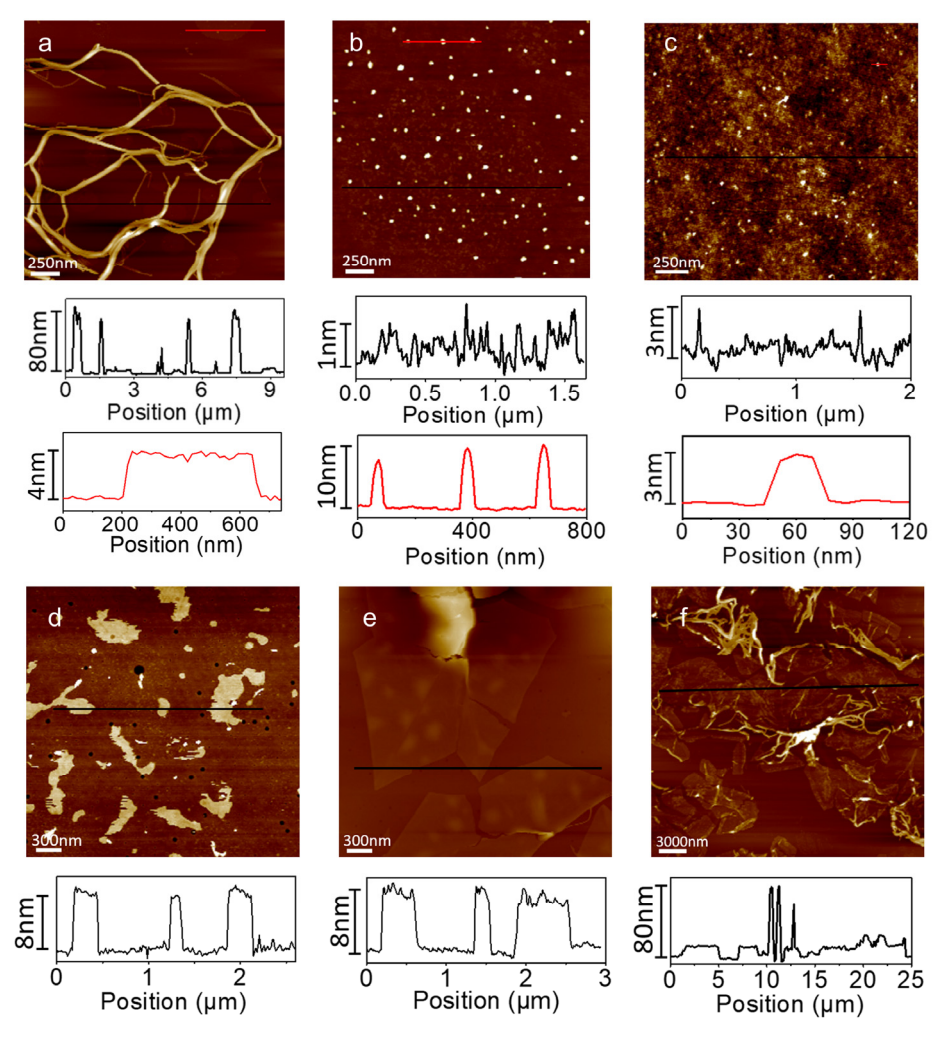


**Figure 4.** Temperature- and MW- dependent of PLLA crystals in ECWS. (a-c) AFM images and the corresponding height profiles of the PLLA crystals formed using 10  $\mu$ L of 0.03 wt.% PLLA solution on the water surface at (a) 0 °C, (b) 60°C, and (c) 80 °C. (d-e) AFM images and the corresponding height profiles of the PLLA crystals formed using 10  $\mu$ L of 0.03 wt.% PLLA solution on the water surface with (d) 0.5, (e) 2, and (f) 100 kDa PLLA.

The mechanism in ECWS is different from polymer crystallization in solution or LB films due to the quasi-2D nature of the system. 1D filaments are the preferred crystal structure, likely due to the pinned polymer chain on the water surface, consistent with the LB cases. However, the freedom of polymer chain diffusion in the surface normal direction complicates the growth behavior, allowing for thicker 1D crystals and 2D lamellae to form. The growth at the interface and in the solution can be decoupled by changing the crystallization conditions, such as the crystallization temperature  $T_c$ . To this end, ECWS of 10  $\mu$ L of 0.03 wt.% PLLA solution at 0, 60, and 80 °C were conducted (results comparable with those shown in **Figure 2b**, which was performed using the same amount of polymer but at 21 °C), and Figure 4 presents AFM images of representative crystal morphologies. Note that evaporation time varied from 10 h for 0 °C to 5 h for 60 and 3h for 80 °C to account for different solvent evaporation rates. Dramatically different morphology can be seen in the figure. At 0 °C, crystals are nearly all 1D, with few round-shaped 2D lamellae in the background. At 21 °C (Figure 2b), biphasic morphology dominates. At 60 °C, relatively isotropic clusters are seen, with an average lateral size of ~60 nm and thickness of  $\sim 10$  nm. In the background, thin rod-shaped crystals with a 0.8-1.1 nm thickness can be seen. At 80 °C, no crystals were collected, indicating the temperature is too high for PLLA crystallization. This series of experiments confirms that PLLA crystallization at the interface and in solution can be tuned by  $T_c$ . At high  $T_c$ , the growth rates of both 1D and 2D crystals are slow, and cluster structures are arrested before large crystals can be developed. The absence of 2D crystals at low  $T_c$  could be due to the longer evaporation time at low  $T_c$ , which allows more complete 1D filament growth before the 2D crystal growth at the interface or the polymer saturation concentration is reached in the solution.

The biphasic nanocrystalline morphology is also polymer *MW*-dependent. To study the effects of chain length on the crystallization of PLLA on the water surface, in addition to the 10 kDa sample previously discussed, 0.5, 2, and 100 kDa PLLA were used, and the results are shown in **Figure 4d-f**. In the case of 0.5 and 2 kDa samples, ECWS yields 2D lamellae with a thickness of ~ 8 nm. No 1D filaments were seen. Biphasic morphology consisting of 2D lamellae and 1D filaments is seen in the 100 kDa sample, similar to the 10 kDa case. The absence of 1D filaments in 0.5 and 2 kDa PLLA might be due to the facile desorption process for shorter chains that leads to statistically less pinned molecules on the water surface. Therefore, no edge-on crystals were observed.

## Conclusion

In summary, we investigated the ECWS of PLLA. Our results show that a biphasic crystalline morphology consisting of 1D filaments and 2D lamellae is formed in ECWS. The 1D filaments are formed by interfacial crystallization of pinned polymer chains at the liquid/liquid interface. 2D lamellae are formed by either loosely pinned polymer chains at the interface or growth into the bulk organic phase, where less confinement on the chain conformation is imposed. The biphasic morphology can be tuned by polymer concentration,

19

crystallization temperature, and polymer MW. Our results demonstrate that ECWS provides a

rich platform to tune polymer crystallization pathways.

ASSOCIATED CONTENT

**Supporting Information** 

The Supporting Information is available free of charge on the ACS Publications website at

DOI: Experimental details, AFM images of ECWS of poly(L,D-lactic acid).

**AUTHOR INFORMATION** 

**Corresponding Author** 

\* Christopher Li, E-mail: chrisli@drexel.edu

ORCID ID: 0000-0003-2431-7099

**Author Contributions** 

QQ conducted the experiments and data analysis. SY assisted TEM experiments. CL directed

the project. The manuscript was written through the contributions of all authors.

**Notes** 

The authors declare no competing financial interest.

**ACKNOWLEDGMENT** 

This research was financially supported by the National Science Foundation CMMI 176262 and DMR 2104968.

## References

- (1) Michell, R. M.; Mueller, A. J. Confined crystallization of polymeric materials. *Prog. Polym. Sci.* **2016**, *54*, 183-213.
- (2) Staub, M. C.; Li, C. Y. Polymer crystallization at liquid-liquid interface. *Polymer Crystallization* **2018**, *I* (4), 10045.
- (3) Li, C. Y. The rise of semicrystalline polymers and why are they still interesting. *Polymer* **2020**, *211*, 123150.
- (4) Hu, W.; Frenkel, D. Effect of Metastable Liquid–Liquid Demixing on the Morphology of Nucleated Polymer Crystals. *Macromolecules* **2004**, *37* (12), 4336-4338.
- (5) Hu, W.; Frenkel, D. Polymer Crystallization Driven by Anisotropic Interactions. *Interphases and Mesophases in Polymer Crystallization III* **2005**, 1-35.
- (6) Wang, H.; Shimizu, K.; Kim, H.; Hobbie, E. K.; Wang, Z.-G.; Han, C. C. Competing growth kinetics in simultaneously crystallizing and phase-separating polymer blends. *J. Chem. Phy.* **2002**, *116* (16), 7311-7315.
- (7) Mitra, M. K.; Muthukumar, M. Theory of spinodal decomposition assisted crystallization in binary mixtures. *J. Chem. Phy.* **2010**, *132* (18), 184908.
- (8) Chuang, W.-T.; Jeng, U. S.; Hong, P.-D.; Sheu, H.-S.; Lai, Y.-H.; Shih, K.-S. Dynamic interplay between phase separation and crystallization in a poly(ε-caprolactone)/poly(ethylene glycol) oligomer blend. *Polymer* **2007**, *48* (10), 2919-2927.
- (9) Schaaf, P.; Lotz, B.; Wittmann, J. C. Liquid-liquid phase separation and crystallization in binary polymer systems. *Polymer* **1987**, *28* (2), 193-200.
- (10) Wang, W.; Qi, H.; Zhou, T.; Mei, S.; Han, L.; Higuchi, T.; Jinnai, H.; Li, C. Y. Highly robust crystalsome via directed polymer crystallization at curved liquid/liquid interface. *Nat. Commun.* **2016**, *7*, 10599, Article.
- (11) Staub, M. C.; Kim, S.; Yu, S.; Li, C. Y. Porous Crystalsomes via Emulsion Crystallization and Polymer Phase Separation. *ACS Macro Lett.* **2022**, *11*, 1022-1027.
- (12) Staub, M. C.; Yu, S.; Li, C. Y. Poly (3-hexylthiophene)(P3HT) Crystalsomes: Tiling 1D Polymer Crystals on a Spherical Surface. *Macromol. Rapid Commun.* **2022**, 2200529.
- (13) Staub, M. C.; Yu, S.; Li, C. Y. Colloidosome-Templated Poly (L-lactic acid) Crystalsomes. *Giant* **2022**, 100124.
- (14) Wang, W.; Staub, M. C.; Zhou, T.; Smith, D. M.; Qi, H.; Laird, E. D.; Cheng, S.; Li, C. Y. Polyethylene nano crystalsomes formed at a curved liquid/liquid interface. *Nanoscale* **2018**, *10* (1), 268-276.

- (15) Qi, H.; Zhou, H.; Tang, Q.; Lee, J. Y.; Fan, Z.; Kim, S.; Staub, M. C.; Zhou, T.; Mei, S.; Han, L. Block copolymer crystalsomes with an ultrathin shell to extend blood circulation time. *Nat. Commun.* **2018**, *9* (1), 3005.
- (16) Staub, M. C.; Li, R.; Fukuto, M.; Li, C. Y. Confined Crystal Melting in Edgeless Poly (lactic acid) Crystalsomes. *ACS Macro Lett.* **2020**, *9* (12), 1773-1778.
- (17) Li, B.; Esker, A. R. Molar mass dependent growth of poly(epsilon-caprolactone) crystals in Langmuir films. *Langmuir* **2007**, *23* (5), 2546-2554.
- (18) Li, B.; Esker, A. R. Blends of poly(epsilon-caprolactone) and intermediate molar mass polystyrene as langmuir films at the air/water interface. *Langmuir* **2007**, *23* (2), 574-581.
- (19) Li, B.; Wu, Y.; Liu, M.; Esker, A. R. Brewster angle microscopy study of poly(epsilon-caprolactone) crystal growth in Langmuir films at the air/water interface. *Langmuir* **2006**, *22* (11), 4902-4905.
- (20) Kumaki, J.; Kawauchi, T.; Yashima, E. Two-Dimensional Folded Chain Crystals of a Synthetic Polymer in a Langmuir–Blodgett Film. *J. Am. Chem. Soc.* **2005**, *127* (16), 5788-5789.
- (21) Takanashi, Y.; Kumaki, J. Significant Melting Point Depression of Two-Dimensional Folded-Chain Crystals of Isotactic Poly(methyl methacrylate)s Observed by High-Resolution In Situ Atomic Force Microscopy. *J. Phys. Chem. B* **2013**, *117* (18), 5594-5605.
- (22) Ni, S.; Yin, W.; Ferguson-McPherson, M. K.; Satija, S. K.; Morris, J. R.; Esker, A. R. Nanoscale surface patterns from 103 single molecule helices of biodegradable poly (L-lactic acid). *Langmuir* **2006**, *22* (14), 5969-5973.
- (23) Ni, S.; Lee, W.; Li, B.; Esker, A. R. Thermodynamics of the liquid expanded to condensed phase transition of poly (L-lactic acid) in Langmuir monolayers. *Langmuir* **2006**, *22* (8), 3672-3677.
- (24) Fuchs, C.; Busse, K.; Flieger, A. K.; Kressler, J. Polymer crystallization on the surface of water or aqueous salt solution. *Chem. Eng. Technol.* **2016**, *39* (7), 1333-1340.
- (25) Hasan, N.; Fuchs, C.; Schwieger, C.; Busse, K.; Dolynchuk, O.; Kressler, J. Crystallization of poly (ε-caprolactone) at the air-water interface studied by IRRAS and GI-WAXS. *Polymer* **2020**, *196*, 122468.
- (26) Iwashima, K.; Yamamoto, T.; Tezuka, Y.; Kumaki, J. Self-Assembly of linear and cyclic polylactide stereoblock copolymers with a parallel and antiparallel chain arrangement distinguishing their directions on a water surface. *Langmuir* **2020**, *36* (22), 6216-6221.
- (27) Watanabe, K.; Kumaki, J. Extended-chain crystallization and stereocomplex formation of polylactides in a Langmuir monolayer. *Polym. J.* **2020**, *52* (6), 601-613.
- (28) Das, A.; El-Tawargy, A. S.; Khechine, E.; Noack, S.; Schlaad, H.; Reiter, G. n.; Reiter, R. Controlling nucleation in quasi-two-dimensional Langmuir poly (l-lactide) films through variation of the rate of compression. *Langmuir* **2019**, *35* (18), 6129-6136.
- (29) Das, A.; Noack, S.; Schlaad, H.; Reiter, G. n.; Reiter, R. Exploring pathways to equilibrate Langmuir polymer films. *Langmuir* **2020**, *36* (28), 8184-8192.

- (30) Hasan, N.; Busse, K.; Haider, T.; Wurm, F. R.; Kressler, J. Crystallization of poly (Ethylene) s with regular phosphoester defects studied at the air—water interface. *Polymers* **2020**, *12* (10), 2408.
- (31) Xie, Q.; Li, B.; Esker, A. R. Phase behavior of poly (ε-caprolactone)-b-poly (tert-butyl acrylate) block copolymer at the air/water interface. *Colloids Surf.*, A **2020**, 587, 124346.
- (32) Khechine, E.; Noack, S.; Schlaad, H.; Xu, J.; Reiter, G.; Reiter, R. Reversible Dehydration–Hydration of Poly (ethylene glycol) in Langmuir Monolayers of a Diblock Copolymer Inferred from Changes in Filament Curvature. *Langmuir* **2023**, *39* (7), 2710-2718.
- (33) Xu, X.; Shao, Y.; Wang, W.; Liu, H.; Zhang, W.; Yang, S. Morphological variation of an LB film of giant amphiphiles composed of poly (ethylene oxide) and hydrophobically modified POSS. *Langmuir* **2021**, *37* (14), 4294-4301.
- (34) Wang, W.-J.; Xu, X.; Shao, Y.; Liao, J.-W.; Jian, H.-X.; Xue, B.; Yang, S.-G. Fractal growth of giant amphiphiles in langmuir-blodgett films. *Chin. J. Polym. Sci.* **2022**, *40* (6), 556-566.
- (35) Zhou, J.; Man, X.; Jiang, Y.; Doi, M. Structure Formation in Soft-Matter Solutions Induced by Solvent Evaporation. *Adv. Mater.* **2017**, *29* (45), 1703769.
- (36) Routh, A. F. Drying of thin colloidal films. Rep. Prog. Phys. 2013, 76 (4), 046603.
- (37) Song, T.; Wu, X.; Xu, J.; Ye, H.; Shi, W. Two-Level Optical Birefringence Created by Evaporation-Induced Polymer Crystallization in Sessile Droplets. *Macromolecules* **2023**, *56* (2), 707-718.
- (38) Li, Y.; Huang, H.; Wang, Z.; He, T. Tuning radial lamellar packing and orientation into diverse ring-banded spherulites: Effects of structural feature and crystallization condition. *Macromolecules* **2014**, *47* (5), 1783-1792.
- (39) Li, Y.; Wang, Z.; He, T. Morphological control of polymer spherulites via manipulating radial lamellar organization upon evaporative crystallization: A mini review. *Crystals* **2017**, *7* (4), 115.
- (40) Tang, Q.; Müller, M.; Li, C. Y.; Hu, W. Anomalous Ostwald Ripening Enables 2D Polymer Crystals via Fast Evaporation. *Phys. Rev. Lett.* **2019**, *123* (20), 207801.
- (41) Qi, H.; Wang, W.; Li, C. Y. Janus Polymer Single Crystal via Evaporative Crystallization. *ACS Macro. Lett.* **2014**, *3*, 675-678.
- (42) Wasanasuk, K.; Tashiro, K.; Hanesaka, M.; Ohhara, T.; Kurihara, K.; Kuroki, R.; Tamada, T.; Ozeki, T.; Kanamoto, T. Crystal structure analysis of poly (l-lactic acid) α form on the basis of the 2-dimensional wide-angle synchrotron X-ray and neutron diffraction measurements. *Macromolecules* **2011**, *44* (16), 6441-6452.
- (43) Strobl, G. From the melt via mesomorphic and granular crystalline layers to lamellar crystallites: A major route followed in polymer crystallization? *Euro. Phys. J., E.* **2000**, *3* (2), 165-183, journal article.
- (44) Strobl, G. Crystallization and melting of bulk polymers: New observations, conclusions and a thermodynamic scheme. *Prog. Polym. Sci.* **2006**, *31* (4), 398-442.

- (45) De Yoreo, J. J.; Gilbert, P. U.; Sommerdijk, N. A.; Penn, R. L.; Whitelam, S.; Joester, D.; Zhang, H.; Rimer, J. D.; Navrotsky, A.; Banfield, J. F. Crystallization by particle attachment in synthetic, biogenic, and geologic environments. *Science* **2015**, *349* (6247).
- (46) Chen, X.; Wang, W.; Cheng, S.; Dong, B.; Li, C. Y. Mimicking Bone Nanostructure by Combining Block Copolymer Self-Assembly and 1D Crystal Nucleation. *ACS Nano* **2013**, *7*, 8251-8257.
- (47) Gleeson, S. E.; Kim, S.; Yu, T.; Marcolongo, M.; Li, C. Y. Insight on the Role of Poly (acrylic acid) for Directing Calcium Phosphate Mineralization of Synthetic Polymer Bone Scaffolds. *ACS Appl. Bio. Mater.* **2022**, *5* (9), 4493-4503.
- (48) Zhu, L.; Cheng, S. Z. D.; Calhoun, B. H.; Ge, Q.; Quirk, R. P.; Thomas, E. L.; Hsiao, B. S.; Yeh, F.; Lotz, B. Crystallization Temperature-Dependent Crystal Orientations within Nanoscale Confined Lamellae of a Self-Assembled Crystalline–Amorphous Diblock Copolymer. *J. Am. Chem. Soc.* **2000**, *122* (25), 5957-5967.
- (49) Lin, M.-C.; Wang, Y.-C.; Chen, J.-H.; Chen, H.-L.; Müller, A. J.; Su, C.-J.; Jeng, U.-S. Orthogonal crystal orientation in double-crystalline block copolymer. *Macromolecules* **2011**, *44* (17), 6875-6884.
- (50) He, W.-N.; Xu, J.-T. Crystallization assisted self-assembly of semicrystalline block copolymers. *Prog. Polym. Sci.* **2012**, *37* (10), 1350-1400.